International Journal of Multiphase Flow 36 (2010) 221–233

Contents lists available at ScienceDirect

International Journal of Multiphase Flow

journal homepage: www.elsevier.com/locate/ijmulflow

Modulation of homogeneous turbulence seeded with finite size bubbles or particles

K. Yeo [a], S. Dong [a,1], E. Climent [b], M.R. Maxey [a,*]

[a] Division of Applied Mathematics, Brown University, Providence, RI 02912, USA
[b] Institut de Mécanique des Fluides de Toulouse, UMR CNRS/INPT/UPS 5502, Allée Camille Soula, 31400 Toulouse, France

ARTICLE INFO

Article history:
Received 23 January 2009
Received in revised form 3 November 2009
Accepted 4 November 2009
Available online 10 November 2009

Keywords:
Dispersed two-phase flow
Homogeneous turbulence
Direct numerical simulation
Particle suspensions

ABSTRACT

The dynamics of homogeneous, isotropic turbulence seeded with finite sized particles or bubbles is investigated in a series of numerical simulations, using the force-coupling method for the particle phase and low wavenumber forcing of the flow to sustain the turbulence. Results are given on the modulation of the turbulence due to massless bubbles, neutrally buoyant particles and inertial particles of specific density 1.4 at volumetric concentrations of 6%. Buoyancy forces due to gravity are excluded to emphasize finite size and inertial effects for the bubbles or particles and their interactions with the turbulence. Besides observing the classical entrapment of bubbles and the expulsion of inertial particles by vortex structures, we analyze the Lagrangian statistics for the velocity and acceleration of the dispersed phase. The turbulent fluctuations are damped at mid-range wavenumbers by the bubbles or particles while the small-scale kinetic energy is significantly enhanced. Unexpectedly, the modulation of turbulence depends only slightly on the dispersion characteristics (bubble entrapment in vortices or inertial sweeping of the solid particles) but is closely related to the stresslet component (finite size effect) of the flow disturbances. The pivoting wavenumber characterizing the transition from damped to enhanced energy content is shown to vary with the size of the bubbles or particles. The spectrum for the energy transfer by the particle phase is examined and the possibility of representing this, at large scales, through an additional effective viscosity is discussed.

1. Introduction

In the context of dispersed two-phase flows in liquids, the study of turbulence seeded with bubbles or small particles is a longstanding topic of research. Engineers involved in the chemical industry, oil extraction or materials handling need to predict both aspects of the coupled dynamics. Of the many applications, there have been a number of recent experiments to investigate the dynamics of drag reduction in boundary layer and channel flows through the injection of gas microbubbles, see for example van den Berg et al. (2005a), Sanders et al. (2006) and Murai et al. (2007). The typical volume fractions encountered in these experiments are in the range of 5–30%. Microbubble drag reduction has been investigated too using various direct numerical simulations as in the studies by Xu et al. (2002), Kawamura and Kodama (2002), Ferrante and Elghobashi (2004), Ferrante and Elghobashi (2005), Lu et al. (2005) and Dong et al. (2005). These illustrate that a range of mechanisms are involved and that the dynamics are a complex interplay of the bubbles with the turbulence and near-wall interactions. Kiger and Pan (2002) have made detailed measurements of the turbulence dynamics for solid particles in horizontal channel flow.

Locally homogeneous turbulence is a simpler context in which to investigate the two-phase flow dynamics and is relevant to the small-scale dynamics of more general turbulent flows. The experiments of Lance and Bataille (1991) provide measurements of the energy spectrum of the turbulent velocity fluctuations with a uniform suspension of bubbles. Changes in the spectrum were noted, as compared to single phase turbulence, that depended on the bubble size and the bubble concentration. These have been followed by more recent experiments by Rensen et al. (2005) and van den Berg et al. (2005b), where a reduction of the spectrum of the energy at large scales and an increase at small scales is observed with a corresponding increase of the dissipation spectrum at the smallest scales. These changes are linked to the bubble size, relative to the Kolmogorov length scale, and the "bubblance" parameter that characterizes the kinetic energy associated with the bubble motion relative to that of the turbulent liquid phase.

Experiments on turbulent two-phase flows are challenging as optical access and phase discrimination are not easy, especially as the volume fraction increases. Computing power has steadily increased over the past two decades making it possible for simulations to approach actual "numerical experiments". Although the direct numerical simulation of homogeneous isotropic turbulence is now well established (Yeung et al., 2006b), only a few numerical

* Corresponding author. Tel.: +1 401 863 1482; fax: +1 401 863 2722.
E-mail address: maxey@dam.brown.edu (M.R. Maxey).
[1] Present address: Department of Mathematics, Purdue University, West Lafayette, IN 47907, USA.

0301-9322/$ - see front matter © 2009 Elsevier Ltd. All rights reserved.
doi:10.1016/j.ijmultiphaseflow.2009.11.001

approaches are able to handle simultaneously all the length scales in a two-phase flow ranging from the surface boundary layers and wakes of individual particles to the largest coherent structures of the flow.

In many two-way coupling simulations, particles have been modeled as point-force source terms in the Navier–Stokes equations, averaged locally over some numerical cell volume of size Δx much larger than a particle. Inherently only a portion of the overall flow is resolved and the disturbance flow generated by individual particles is modeled as for Boivin et al. (1998) and Hwang and Eaton (2006). The dispersed phase motion is simulated in a Lagrangian framework using a particle tracking, force balance equation to predict each particle trajectory. The fluid forces on a particle are explicitly estimated in terms of a slip velocity between the particle motion and the resolved (larger scale) flow field of the surrounding fluid. The underlying assumption is that the typical size of the particles or bubbles is significantly smaller than all the significant scales of the turbulent fluid flow. This approach is relevant when the turbulent modulation is induced by collective effects and when direct hydrodynamic interactions between particles can be neglected. Such conditions may occur for very low volume fractions of the dispersed phase. Even with these limitations, some basic features have been revealed on the modulation of homogeneous turbulence in gas–solid flows, see for example (Squires and Eaton, 1990; Elghobashi and Truesdell, 1993); Boivin et al. (1998); (Druzhinin and Elghobashi, 1999). Similarly, corresponding results have been obtained for bubble-laden turbulence (Mazzitelli and Lohse, 2003; Mazzitelli et al. (2003)). The results of the latter simulations are in qualitative agreement with the experiments (Rensen et al., 2005; van den Berg et al., 2005b) as summarized by van den Berg et al. (2006).

In many liquid–solid flows, the typical Reynolds number of the carrying flow is often high and the smallest scales of the velocity field are generally smaller than or comparable to the particle (or bubble) diameter. In these contexts, point-force approximations are less applicable because the scale separation is no longer effective. Only a few studies have considered the finite size of the particulate phase in a turbulent flow. Sundaram and Collins (1999) among others took this constraint into account by including elastic collisions between particles but the hydrodynamic forcing terms were still assumed to be local point (Dirac delta) functions. More recently, ten Cate et al. (2004) carried out a fully resolved simulation of a liquid–solid turbulent suspension. By means of the lattice-Boltzmann method (LBM) they simulated moderately concentrated two-phase flows, at volume fractions of 2–10%, in a sustained homogeneous turbulence. Finite size particles with a solid to fluid density ratio varying from 1.15 to 1.73 generated perturbations in the three-dimensional homogeneous turbulent flow. Fluctuating motions were observed to be enhanced at small scales and the energy spectra showed a weak reduction in the lower wavenumber content. The range of scales involved in the dissipation of fluid kinetic energy are clearly increased when particles are seeded in the flow. Using a new modeling approach, namely PHYSALIS, Zhang and Prosperetti (2005) simulated the modulation of decaying homogeneous isotropic turbulence seeded with particles four times larger than the Kolmogorov scale. Neglecting the effect of gravity, they showed in their preliminary study that the presence of particles enhances dissipation whereas the turbulence decay rate of the turbulence is slightly increased.

At low volume fractions a characteristic feature of particle motion in turbulence is for local particle accumulations to develop in response to the local vorticity or rate of strain in the flow. This depends on the inertial response time of the particle and is generally strongest for small particles when the response time matches the Kolmogorov time scale (Wang and Maxey, 1993a,b). Particles denser than the surrounding fluid tend to collect in regions of high rates of strain, while particles (or bubbles) less dense tend to collect in regions of high vorticity and lower fluid pressure (Maxey, 1987). Calzavarini et al. (2008) have shown that the tendency for bubbles to cluster is significantly stronger than for denser particles. For larger particles, where the response time of the particle falls within the inertial sub-range, one may expect particles to exhibit clustering in response to turbulent motions with time scales comparable to those of the particle response time. This has been explored through numerical simulations for gas–solid turbulent flows by Yoshimoto and Goto (2007), where the response time is large compared to Kolmogorov scales but the physical dimensions of the particles remain very small. In general though, there is both an effective *temporal* filtering of the particle response to the turbulence and an effective *spatial* filtering associated with the finite size of the particle in comparison to the spatial scales of the turbulence, as noted for example by Xu and Bodenschatz (2008). These are still open questions.

Recent experiments for isolated particles by Qureshi et al. (2007), Volk et al. (2008) and Xu and Bodenschatz (2008), based on earlier work by Voth et al. (2002), have investigated the response of finite size particles to isotropic turbulence. These experiments cover almost neutrally buoyant particles, bubbles and particles with specific density ratios up to 1.4. The experiments are able to achieve a higher Reynolds number, and hence establish more of an inertial sub-range, than is generally possible in numerical simulations. By examining the particle acceleration statistics it is generally observed that for neutrally buoyant particle with diameters five times the Kolmogorov scale or less the response is essentially the same as a Lagrangian fluid element. For larger particles there is a transition in the response as the diameter falls within the inertial sub-range. Qureshi et al. (2007) observe that for particle diameters larger than fifteen times the Kolmogorov scale, the acceleration variance of neutral particles is consistent with an inertial range scaling.

In this paper we use the force-coupling method (FCM) to provide a detailed representation of particles in the flow and investigate the modulation of homogeneous isotropic turbulence induced by spherical bubbles, neutrally buoyant particles and slightly inertial particles at volume fractions of 3–6%. We exclude the effects of gravitational settling or buoyancy and focus on the effects associated with the finite size (and volume) of the particles, within the range of 6–12 Kolmogorov scales in diameter. The force-coupling method provides a bridge between the point-particle methods used for gas–solid flows and the more detailed resolution of LBM, immersed boundary method or PHYSALIS simulations. FCM is an efficient scheme for simulating large numbers of small particles in dispersed two-phase flow and has been applied previously to simulations of microbubble drag reduction, (Xu et al., 2002) and sedimentation at finite Reynolds numbers (Climent and Maxey, 2003).

The paper is organized as follows. First, we summarize the basic features of the force-coupling method and the numerical parameters for the simulation of the homogeneous turbulent two-phase flow. Initial observations about the bubble or particle distributions and dispersion are then noted. We follow by a discussion of the results on turbulence modulation by bubbles, neutral or inertial particles. The last two sections are devoted to Lagrangian statistics of the dispersed phase and to comments about the features observed. Our goal is not to provide definitive answers to the dynamics of two-phase flow in homogeneous turbulence but to point to the many open issues that still need further investigation.

2. Simulation methods

2.1. Force-coupling method

The coupled two-phase flow dynamics of the bubbles or particles and the turbulence is simulated using the force-coupling method, described in Maxey and Patel (2001), Lomholt et al. (2002) and Lomholt and Maxey (2003). FCM is based on a low-order, finite force multipole representation for the influence of the particles in the flow. The fluid is assumed to fill the entire simulation domain, including the volume occupied by the bubbles or particles. The presence of the dispersed phase is then represented by a finite force monopole and a force dipole that generate a body force distribution $\mathbf{f}(\mathbf{x},t)$ on the fluid. The volumetric velocity field $\mathbf{u}(\mathbf{x},t)$ and pressure $p(\mathbf{x},t)$ are solutions of the mass conservation Eq. (1) for an incompressible fluid

$$\nabla\cdot\mathbf{u}=0 \tag{1}$$

and satisfy the Navier–Stokes Eq. (2)

$$\rho\frac{D\mathbf{u}}{Dt}=-\nabla p+\mu\nabla^2\mathbf{u}+\mathbf{f}(\mathbf{x},t) \tag{2}$$

where μ and ρ are the fluid viscosity and density. The body force due to the presence of N bubbles or particles can be written as the sum of two contributions

$$f_i(\mathbf{x},t)=\sum_{n=1}^{N}F_i^{(n)}\Delta(\mathbf{x}-\mathbf{Y}^{(n)}(t))+G_{ij}^{(n)}\frac{\partial}{\partial x_j}\Delta'(\mathbf{x}-\mathbf{Y}^{(n)}(t)) \tag{3}$$

where $\mathbf{Y}^{(n)}$ is the position of the nth spherical bubble or particle, $\mathbf{F}^{(n)}$ is the force experienced by the fluid and $\mathbf{G}^{(n)}$ is the strength of the force dipole.

The spatial distribution of the force monopole acting on the fluid is specified by a spherical Gaussian envelope $\Delta(\mathbf{x})$ as

$$\Delta(\mathbf{x})=(2\pi\sigma^2)^{-3/2}\exp(-\mathbf{x}^2/2\sigma^2) \tag{4}$$

The length scale σ is set in terms of the bubble radius a as $a/\sigma=\sqrt{\pi}$ (Maxey and Patel, 2001). This ensures, amongst other results, that the particle velocity matches the Stokes settling velocity under low particulate Reynolds number and captures the Faxen correction for motion in a nonuniform flow. The velocity of each bubble or particle $\mathbf{V}^{(n)}(t)$ is obtained by forming a local average of the volumetric velocity field over the region occupied by the bubble

$$\mathbf{V}^{(n)}(t)=\int_D\mathbf{u}(\mathbf{x},t)\Delta(\mathbf{x}-\mathbf{Y}^{(n)}(t))\,d^3\mathbf{x} \tag{5}$$

Finally, trajectories are determined by numerical integration of the equation

$$\frac{d\mathbf{Y}^{(n)}(t)}{dt}=\mathbf{V}^{(n)}(t) \tag{6}$$

If m_P (m_B for bubbles) and m_F denote the mass of a particle and the mass of displaced fluid, respectively, the force experienced by the fluid due to the presence of the particle is

$$\mathbf{F}^{(n)}=(m_P-m_F)\left(\mathbf{g}-\frac{d\mathbf{V}^{(n)}}{dt}\right)+\mathbf{F}_C^{(n)} \tag{7}$$

This force is the sum of the net external force due to buoyancy of the particles (or bubbles), the inertia excess over the corresponding volume of displaced fluid due to the density difference and a contact force between particles. In the present paper we neglect the effect of gravity $\mathbf{g}$ and focus on the inertial interactions between the phases as well as the effects of finite particle size. These conditions may be achieved in experiments under microgravity or where the terminal settling velocity is very small compared to the turbulent velocity scales. For gas bubbles in liquids, the mass is negligible ($m_B\ll m_F$) and the monopole term $m_F d\mathbf{V}/dt$ represents the primary interphase coupling through momentum transfer. Results on bubbly turbulence will be compared to simulations with neutral particles ($m_P=m_F$), where only the force dipole contribution $G_{ij}^{(n)}$ is nonzero, and also with inertial particles ($m_P>m_F$).

The term $\mathbf{F}_C^{(n)}$ represents the effects of short-range hydrodynamic interactions and a rigid-body contact force that prevents bubbles or particles from overlapping. In the present simulations, and as in Xu et al. (2002), we assume that bubbles are small enough that they remain spherical and due to surface contamination respond approximately as rigid spheres (no-slip boundary condition). Also, when bubbles come into contact they do not coalesce but eventually separate again. We use an effective repulsion or contact force between bubble or particle surfaces. The contact force for each pair i and j, is a function of the relative position vector $\mathbf{x}_{ij}=\mathbf{Y}^{(i)}-\mathbf{Y}^{(j)}$ and the distance $r_{ij}=\|\mathbf{x}_{ij}\|$. If $r_{ij}<R_{ref}$, the cut-off length scale for the barrier, then the contact force acting on particle i due to particle j is

$$\mathbf{F}_C^{ij}=\frac{F_{ref}}{r_{ij}}\left[\frac{R_{ref}^2-r_{ij}^2}{R_{ref}^2-4a^2}\right]^2\mathbf{x}_{ij} \tag{8}$$

Otherwise the contact force is zero. This force acts along the line of centers of each pair, it is elastic and conserves momentum.

We fixed the force scale as $F_{ref}=m_F(\nu_K/\tau_K)$ (see later in the section for definitions and the values in Table 1) and the cut-off scale as $R_{ref}/2a=1.2$ in the present simulations. The actual value of the force barrier during a collision is set in response to the proximity of the bubbles (or particles) and the relative turbulent motion leading to the contact. The total force is obtained through a pairwise summation,

$$\mathbf{F}_C^{(i)}=\sum_{i\neq j}\mathbf{F}_C^{ij} \tag{9}$$

It is important to include these collisions or contact effects in order to maintain the volume fraction of the dispersed phase. Further details on these short-range interactions are given in Dance et al. (2004). At higher volume fractions it is necessary to provide a more detailed representation including viscous lubrication forces and solid-body contact forces. In principle, viscous lubrication forces will prevent contact of perfectly smooth particles but contact occurs in practice through surface roughness and other variations. Tests were made, varying the magnitude of the force F_{ref} and the cut-off distance R_{ref}. The results presented here were found to be insensitive to the specific value of F_{ref} within a broad working range. There was a more obvious effect of varying R_{ref} but for the chosen value this was still not significant, especially at the average concentration levels of 6% or less considered here. Any transient overlap between particles was negligible.

The symmetric part of the force dipole $G_{ij}^{(n)}$, the stresslet term, is set through an iterative procedure to ensure that the strain-rate within the fluid volume occupied by the dispersed phase is zero (when spatially averaged on the appropriate bubble or particle scale σ'). The instantaneous, volume integrated, rate of strain is evaluated through the equation

$$S_{ij}=\frac{1}{2}\int\left(\frac{\partial u_i}{\partial x_j}+\frac{\partial u_j}{\partial x_i}\right)\Delta'(\mathbf{x}-\mathbf{Y}^{(n)}(t))d^3\mathbf{x} \tag{10}$$

The condition is then that S_{ij} is zero for each particle. The length scale of the envelope σ' associated with Δ' is specified as $a/\sigma'=(6\sqrt{\pi})^{1/3}$, or approximately 2.20, see Lomholt and Maxey (2003). The details of the iterative solver used are given by Dance and Maxey (2003) and this converged typically within three iterations.

Table 1
Simulation parameters of the sustained homogeneous isotropic turbulence (single phase flow). Parameter definitions are given in Sections 2.2 and 2.3. The standard Kolmogorov velocity, length and time scales are v_K, η and τ_K.

Grid	u'	ϵ	ν	Re_λ	λ	T_e	$u'T_e$	η	τ_K	v_K	$k_{max}\eta$
192^3	19.8	5562	0.12	58.7	0.356	0.070	1.39	0.0236	0.0046	5.08	2.1

For a laminar flow the additional stresslet term leads to an enhanced viscous dissipation. Even for a neutrally buoyant particle moving with the surrounding fluid, any local rate of strain in the flow will be deflected around the particle, see for example Fig. 3 of Lomholt and Maxey (2003), leading to a locally higher rate of strain and dissipation near the particle. As described in Section 4.11 of Batchelor (1967), this may be represented by an effective viscosity in a suspension of many particles. Summing the stresslet contributions in a dilute sheared suspension of rigid spheres gives the classical Einstein estimate of the effective viscosity under conditions of Stokes flow,

$$\mu_{eff} = \mu(1 + 2.5\phi + \alpha\phi^2) \tag{11}$$

where ϕ is the volume fraction of the particles. The second-order coefficient α depends on the specific particle configuration (Batchelor and Green, 1972). These effects are captured by FCM at low volume fractions, and at larger volume fractions when the appropriate lubrication forces are included (Abbas, 2008; Yeo and Maxey, 2010).

The anti-symmetric part of the dipole corresponds to the sum of an external torque, $\mathbf{T}_{ext}$ and the excess inertia for rotation of the particle (I_P) or bubble (I_B) over the corresponding, appropriately chosen, volume of fluid (I_F) as given by

$$\mathbf{T}^{(n)} = \mathbf{T}^{(n)}_{ext} - (I_P - I_F)\left(\frac{d\mathbf{\Omega}^{(n)}}{dt}\right) \tag{12}$$

$d\mathbf{\Omega}/dt$ is the rate of variation of the particle (or bubble) rotation rate and the angular velocity $\mathbf{\Omega}$ is evaluated in Eq. (13) as

$$\mathbf{\Omega}^{(n)}(t) = \frac{1}{2}\int \{\nabla \times \mathbf{u}(\mathbf{x}, t)\}\Delta'(\mathbf{x} - \mathbf{Y}^{(n)}(t))d^3\mathbf{x} \tag{13}$$

No external torques are applied to the particles in the present simulations, $\mathbf{T}_{ext} = 0$. The rotation rate of a particle changes in response to the viscous stresses exerted by the surrounding fluid, summed over the particle surface, and the moment of inertia of the particles. Neutrally buoyant particles respond quickly and their rotation rate is in equilibrium with the rotation rate of the surrounding fluid at that length scale. The (rigid) bubbles would show the largest discrepancy due to differences in inertia but were found still to come to equilibrium quite quickly. We monitored the amplitude of both symmetric and anti-symmetric parts of the dipole $G^{(n)}_{ij}$ in selected simulations of bubble motion involving both motion in a single vortex and in stationary isotropic turbulence. The antisymmetric contribution is significantly weaker than the stresslet term. It represents less than 8% when averaged over all bubble trajectories. While (12) is correct in principle the specification of I_F for FCM is not trivial. We decided to exclude this small effect rather than introduce a possibly inaccurate fluctuating term in the simulations. Hence throughout the simulations $\mathbf{T}^{(n)} = 0$.

Examples of the application of FCM to the motion of particles at low to moderate, finite Reynolds numbers, together with comparisons to fully resolved direct numerical simulations, are given in Liu et al. (2002) and Maxey et al. (2006). A discussion of the response to unsteady flow conditions, including the ability of FCM to capture Basset history forces, is reported in Maxey (1999). The formulation of FCM provides a consistent energy budget for both the fluid and particle phases. Viscous dissipation of fluid kinetic energy is evaluated by integration over the whole domain including the volume occupied by the particles. This is required since the representation of the particles involves a spatial smoothing or filtering of the near-surface conditions for each particle and the interior of the particle volume remains an active part of the flow (Maxey and Patel, 2001; Lomholt and Maxey, 2003).

2.2. Turbulent flow

The flow is simulated in a fully periodic domain, of size $2\pi \times 2\pi \times 2\pi$, using a Fourier pseudo-spectral code. The turbulent flow is sustained by a random forcing at low wavenumbers to achieve a statistically stationary state. The simulation procedure is similar to that used by Wang and Maxey (1993b) with the random forcing term applied over a shell of small wavenumbers (Eswaran and Pope, 1988). The forcing term is applied to nonzero wavenumbers in the range $0 < k \leqslant 3$. This unsteady forcing will drive the large length scales of the flow. When a sufficiently large separation between production and dissipation scales occurs the small-scale structures exhibit the universal characteristics of a turbulent flow. Basic data on the single phase turbulence are given in Table 1. The simulations are based on a 192^3 grid resolution, for which $k_{max}\eta = 2.1$. Simulations on a 128^3 grid yielded the same results but with a lower resolution, $k_{max}\eta = 1.4$. Both are adequately resolved, with $k_{max}\eta > 1$ (Sundaram and Collins, 1997). The forcing parameters are the same in all simulations and a balance between the average energy input from the forcing and the viscous dissipation rate ϵ is achieved.

The turbulent kinetic energy K, or turbulence intensity u', is obtained by averaging over space and time after the initial transient (two to three integral time scales) necessary to develop stationary turbulence. This can be also evaluated in the spectral space by integrating the energy spectrum function $E(k)$ as

$$K = \frac{3}{2}u'^2 = \frac{1}{2}\langle u'_i u'_i \rangle = \int_0^{k_{\max}} E(k)dk \tag{14}$$

The rate of kinetic energy dissipation per unit volume, ϵ is balanced by the volumetric power input of the turbulence forcing and it is directly evaluated by integration of the dissipation spectrum $D(k)$ over all the wavenumbers

$$\epsilon = \int_0^{k_{\max}} D(k)dk = 2\nu\int_0^{k_{\max}} k^2 E(k)dk \tag{15}$$

where $\nu = \mu/\rho$ is the kinematic viscosity. Energy and dissipation spectra for the single phase turbulence are shown in Section 4. Among others, two typical length scales characterize the turbulent fluid motion, namely the Taylor microscale, λ, defined by $\lambda^2 = 15\nu u'^2/\epsilon$, and the Kolmogorov length scale, η, defined by $\eta = (\nu^3/\epsilon)^{1/4}$. The Reynolds number of the single phase flow, based on the Taylor microscale $Re_\lambda = u'\lambda/\nu$ is 59.

2.3. Simulation parameters

The primary group of simulations are for bubbles (B), neutrally buoyant particles (N) and inertial solid particles (S) at a volume fraction of approximately 6%. The parameters for these simulations are listed in Table 2. Two particle or bubble sizes are considered, with particle radius $a = 0.1305$ or 0.091. For the larger particles,

Table 2
Parameters of the flow simulations: Bubbles ($B, m_B = 0$), Neutrally buoyant particles ($N, m_P = m_F$) and Solid particles ($S, m_P = 1.4m_F$). Particle radius $a = 0.1305$ (1) or $a = 0.091$ (2). All simulations include force monopole (M) and dipole terms (D), except $S2$–M which is based on the monopole only. Parameter definitions are given in Sections 2.2 and 2.3; N_P is the number of particles.

Case	Grid	N_P	Re_λ	u'	ϵ	a/η	a/λ	St	τ_i/τ_K
$B1$	128^3	1600	59.7	20.18	5827	5.59	0.37	0.23	3.5
$B2$	192^3	4508	59.2	20.14	5876	3.90	0.26	0.11	1.7
$N1$	128^3	1600	57.3	19.44	5436	5.50	0.37	0.68	10.1
$N2$	192^3	4508	58.7	19.77	5574	3.84	0.26	0.33	5.0
$S1$	128^3	1600	57.0	19.44	5490	5.51	0.37	0.87	12.8
$S2$	192^3	4508	57.3	19.54	5552	3.84	0.26	0.42	6.3
$S2$–M	192^3	4508	58.3	19.78	5629	3.86	0.26	0.42	6.3

$N = 1600$ and corresponds to a volume fraction of 6.0% while for the smaller particles, $N = 4508$ and corresponds to a volume fraction of 5.7%. In order to resolve the motion of the particles using FCM, the minimum spatial resolution should be between 5 and 6 grid points to a particle diameter to accurately represent the effect of both the force monopole and dipole terms. The larger particles are simulated adequately with a numerical grid of 128^3 points for which then $a/\Delta x = 2.66$. The smaller particles are simulated on a 192^3 grid for which $a/\Delta x = 2.78$.

Particles or bubbles are initially seeded at random positions in the homogeneous turbulent flow and statistics are computed after a transient period, typically one or two integral time scales. The particle concentrations remain uniform on average but local fluctuations develop in response to the turbulence. These fluctuations depend on the relative inertial response time of the particles (or bubbles) to the turbulence time scales. The bubble response time is defined in terms of the mass of displaced fluid and the added-mass effect. The Stokes drag law provides a convenient reference estimate for defining the response time, so that $\tau_B = a^2/9\nu$. For inertial solid particles, with relative density $\rho^* = \rho_P/\rho$, the particle relaxation time scale is $\tau_P = 2(\rho^* + 1/2)a^2/9\nu$ and $\rho^* = 1$ for neutral particles (index N) while $\rho^* = 1.4$ for the inertial particles (index S). We define the Stokes number St by comparing τ_B (or τ_P) to the turbulence time scale $T_e = u'^2/\epsilon$, for the large eddy turnover time or eddy lifetime. This definition does not account for any specific modification to the drag law based on instantaneous Reynolds number, but it is appropriate as an a priori estimate for the bubble or particle response to the turbulence in the absence of buoyancy effects. The Stokes number (16) is also equivalent to comparing the bubble or particle radius a to the Taylor microscale λ, since the rate of viscous dissipation per unit mass ϵ is equal to $15\nu u'^2/\lambda^2$ in homogeneous isotropic turbulence,

$$St = \frac{\tau_i}{T_e} = \frac{5}{3}\alpha_i \frac{a^2}{\lambda^2} \tag{16}$$

In (16) the coefficient α_i is equal to 1 for bubbles (B), 3 for neutral particles (N) and 3.8 for inertial particles (S).

The primary data related to the two-phase simulations are summarized in Table 2. The case index is a combination of the particle type (B, N or S) and the size of the particle (1 or 2) corresponding respectively to a radius $a = 0.1305$ or $a = 0.091$. The particles or bubbles are larger than the Kolmogorov scale with a length scale ratio a/η varying from 3.8 to 5.6. On the other hand, they are smaller than the Taylor microscale, typically from $\lambda = 2.7a$ to $\lambda = 4a$ meaning that the disperse phase will be interacting with the full range of the most energetic structures of the turbulent flow. For all the simulations, the Stokes number St is low or moderate, based on the estimate (16) using the integral time scale. We also provide the values of the particle relaxation time compared to the Kolmogorov time scales.

3. Initial results

A basic feature of microbubble dispersion is a preferential accumulation of bubbles in regions of high vorticity. This is a consequence of the absence of inertia of the bubble itself (Magnaudet and Eames, 2000). In a turbulent flow, bubbles are likely then to collect within the cores of vortex tubes that may form in the flow. In the present simulations, the dispersion of bubbles is driven by the force monopole, $\mathbf{F} = -m_F d\mathbf{V}/dt$. As compared to point-particle tracking schemes, the effects of Basset history forces, added-mass or lift forces are implicit to the present simulations. We investigated the time evolution of levels of the fluid vorticity $\boldsymbol{\omega}$ at the Lagrangian locations of bubbles or particles, based on the point values at the center. Initially, bubbles were seeded randomly within the domain and the root mean square (rms) vorticity level at the bubble locations matches the average value in the turbulent flow. As time goes on (typically, less than one integral time scale), bubbles tend to collect in the vortex structures of the flow. Instantaneous snapshots of the flow show that bubbles are clearly accumulated in high vorticity regions, see Fig. 1, where a planar section of the flow is shown together with the bubbles in that section and the local value of the enstrophy ω^2. We verified that the accumulation regions indeed correspond to vortex cores as defined by Jeong and Hussain (1995) using the λ_2 eduction scheme.

Fig. 2 shows a sample of the time-history for the rms vorticity fluctuations following bubbles or particles. Again these were evaluated from point data taken on a 128^3 grid simulation, for cases $B1$ and $S1$. With either the monopole term only ($B1$–M) or the usual monopole and stresslet terms ($B1$), the vorticity fluctuations following the bubbles are significantly higher. The baseline variations for the single phase flow reflect the variability of the energy input, and the dissipation, given the random forcing scheme that sustains the turbulence. The solid particles ($S1$) have a somewhat reduced level of vorticity fluctuations. The same features are reflected in the Lagrangian data presented later in Table 5 for the rms fluctuations in the angular velocity $\boldsymbol{\Omega}$ of a particle or bubble, evaluated from (13). The accumulation level depends primarily at low concentrations on the finite size of the bubble and the relative relaxation time scale τ_B/τ_K, becoming strongest when $\tau_B/\tau_K \sim 1$ (Wang and Maxey, 1993a).

Contact forces between particles (or bubbles) will tend to limit any increase in local particle concentration, even before the close-packing limit is reached. In the present simulations, the force barrier (8) is used to represent the short-range interactions between the particles as described in Section 2.1. The rate of collisions for solid particles in a liquid turbulent flow are considered in detail by ten Cate et al. (2004) and by Brunk et al. (1998) and we do not address these issues here. Contact forces, and other short-range interactions, do contribute to the overall particle-phase stress. They may also potentially alter the rate of turbulent diffusion of bubbles (or particles) in the flow at finite volume fractions.

In our initial investigations, we examined the interactions of bubbles and turbulence and determined the long-term dispersion coefficient D for several different bubble sizes at two different void fraction levels, 3% and 6%. The parameters for this separate set of simulations are given in Table 3. Note that the dispersion coefficient is most strongly influenced by the larger scales in the turbulence and as such may be influenced by the low wavenumber random forcing used to sustain the flow. In the usual way, each bubble was tracked from an initial position $\mathbf{Y}(0)$, at some initial reference time, and the relative displacement recorded. According to standard theory of particle dispersion in homogeneous, stationary turbulence (Taylor, 1921) the mean square relative displacement, choosing one directional component, will converge as $t \to \infty$ to give

$$\langle [Y_1(t) - Y_1(0)] V_1(t) \rangle = D \tag{17}$$

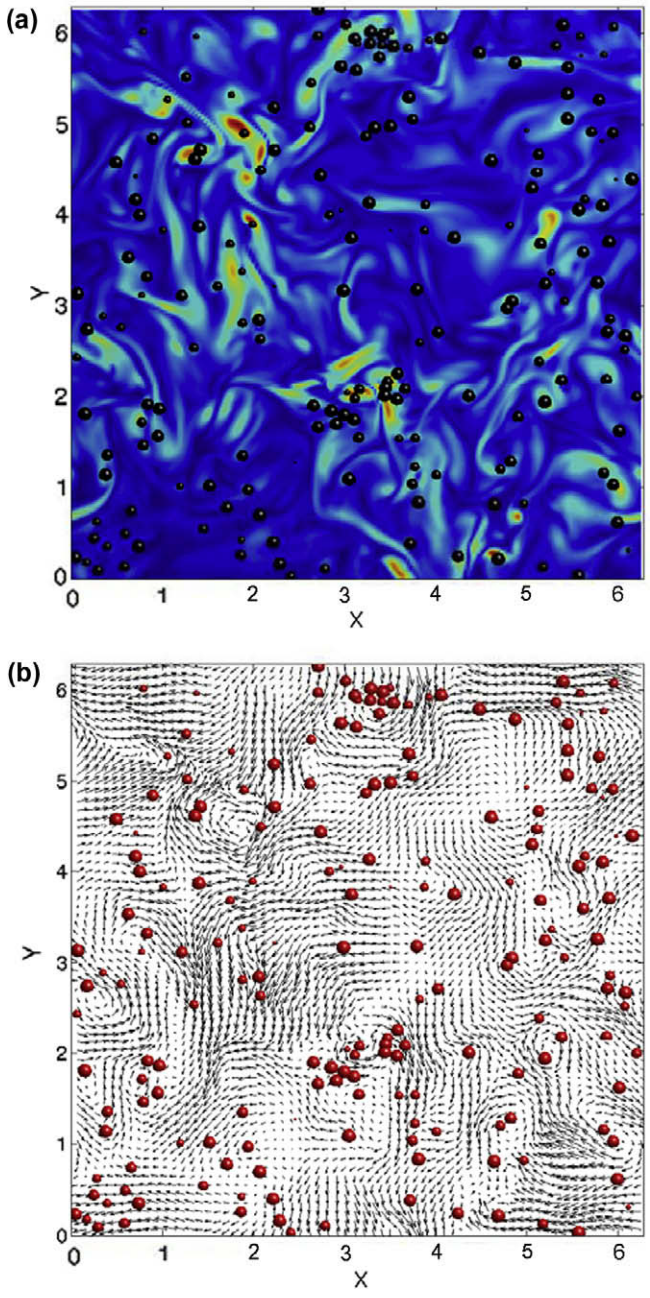

Fig. 1. (Color online) (a) Instantaneous bubble positions and enstrophy level (case *B*1). Bubbles are displayed with their actual size in the planar slice, with high enstrophy levels shown as white. (b) Corresponding view of bubble positions and fluid velocity, shown by the vector arrows.

This may be written as $D = \langle V_1^2 \rangle T_L$, where T_L is the Lagrangian integral time scale. The dispersion coefficient D was evaluated from the equivalent long term value of

$$\langle [Y_1(t) - Y_1(0)]^2 \rangle / 2t = D \tag{18}$$

In all cases, the data is calculated using (18) with a time-averaged estimate from $t = 0.3$–1.5, corresponding to an interval in excess of $17T_e$. This provided a stable estimate of the dispersion coefficient with lower statistical fluctuation.

The results for the bubble dispersion coefficient are given in Table 3. All these results were obtained using the 192^3 grid as given in Table 1. Additional bubble sizes, beyond those given in Table 2 were included and the details are given in Table 3. Only the force monopole term in the FCM was used in this set of simulations so as to focus specifically on the effects of the bubble collisions on dispersion. At the lower concentration, 3% void fraction, there is only a small variation in the dispersion coefficient with bubble size as shown by the results for cases MB5–MB8. The average value of $D/u'^2T_e = 0.40 - 0.41$ may be compared with the value of 0.43 reported by Yeung and Pope (1989) for the dispersion of Lagrangian fluid particles. Their simulations were made using a similar forcing scheme to sustain stationary isotropic turbulence and the Reynolds number, $Re_\lambda = 63$, is close to the present value. The dispersion coefficients may also be compared to standard estimates of the eddy viscosity, which according to a standard $k - \epsilon$ model is $\nu_T/u'^2T_e = 9C_\mu/4$ (Pope, 2000). The coefficient $C_\mu = 0.09$ and so the ratio is 0.202 implying that the turbulent Schmidt number for bubble dispersion is about 0.5.

At the lower void fraction, the rms velocity fluctuation of the bubbles, defined as $V' = \langle V_1^2 \rangle^{1/2}$, varies between $0.90u'$ for the largest bubbles and $0.94u'$ for the smallest. The integral time scale will be longer for the larger bubbles, due to the greater inertia effect, and this in part compensates for the reduction in the velocity fluctuations so that the dispersion overall shows less variation. At the higher bubble concentration of 6%, the rms velocity fluctuation shows a similar variation. The dispersion coefficient however shows a more noticeable variation, with the dispersion for the larger bubbles being reduced and that of the smaller bubbles increased. This may be attributed to the effects of bubble-bubble

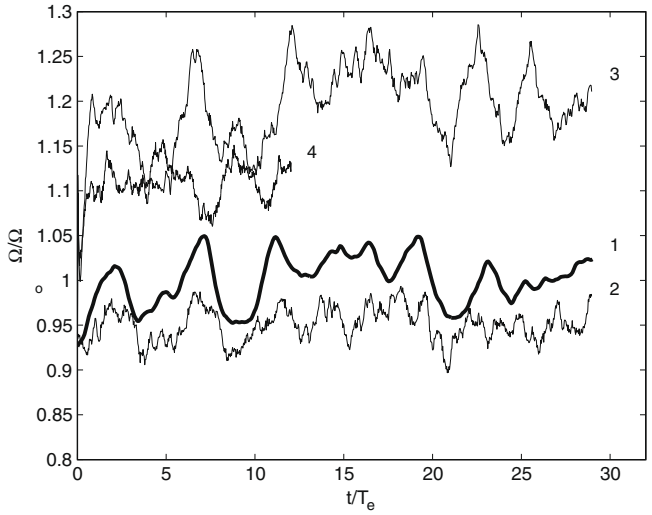

Fig. 2. Sample Lagrangian time-history of rms vorticity fluctuations following the bubbles or particles, corresponding to cases *S*1 and *B*1: (1) single phase flow; (2) particles (*S*1); (3) bubbles simulated with force monopole only (*B*1–*M*); and (4) bubbles (*B*1).

Table 3
Results for bubble dispersion and pressure due to collision forces. Simulations on 192^3 grid with only the force monopole term for FCM. Bubble void fraction ϕ is 3.0% or 6.0% .

Case	a	N	ϕ	a/λ	τ_B/τ_K	D/u'^2T_e	V'/u'	$P_B/\phi^2u'^2$
MB1	0.19	517	0.06	0.535	7.4	0.360	0.900	1.50
MB2	0.1305	1600	0.06	0.366	3.5	0.409	0.928	1.26
MB3	0.09	4866	0.06	0.254	1.7	0.436	0.946	1.02
MB4	0.0725	9322	0.06	0.204	1.1	0.441	0.956	0.88
MB5	0.19	259	0.03	0.535	7.4	0.41	0.90	–
MB6	0.1305	800	0.03	0.366	3.5	0.40	0.93	–
MB7	0.09	2433	0.03	0.254	1.7	0.40	0.93	–
MB8	0.0725	4661	0.03	0.204	1.1	0.41	0.94	–

collisions at the higher void fraction. These collisions will tend to limit the long-term correlation of the bubble motion in (18) and would tend to reduce the integral time scale for dispersion due to turbulence. The collisions may further augment the velocity fluctuations at higher frequencies. The determining factor is the average time interval between collisions for a bubble as compared to the turbulence time scale T_e. The collision rate is higher for larger particles (or bubbles) in this size range as reported by ten Cate et al. (2004). The collision rate also scales with the concentration as ϕ^2, so that these effects will be more pronounced as the void fraction increases.

The bubble-bubble collisions also contribute to the particle-phase stress on the fluid. The contact barrier (8) is a conservative force, acting along the line of centers, and in the absence of a preferred orientation, this leads to an effective dispersive pressure field P_B. This effect is well known in the context of granular flows and is referred to as the Bagnold dispersive stress (Campbell, 1990), and is encountered too in fluidized beds. Collision-induced pressures in solid–liquid flows have been measured by Zenit et al. (1997) and the different possible representations of this effect in bubble column dynamics are discussed by Minev et al. (1999). The dispersive pressure field depends on both the strength of the contact forces and the frequency of bubble contacts. Batchelor (1988) proposed a model for the mean pressure as

$$P_B = \rho u_0^2 \phi \frac{\phi}{\phi_*}\left(1 - \frac{\phi}{\phi_*}\right) \tag{19}$$

where u_0 is an appropriate velocity scale. In the limit of close packing, $\phi = \phi_*$, the dispersive pressure drops to zero, while at low void fraction it is proportional to ϕ^2. Although there is considerable scatter in the measurements reported by Zenit et al. (1997) their results do support this trend for the normalized pressure with a peak value at void fractions of about 30%.

In the present simulations of homogeneous turbulence with uniform seeding of the bubbles the ensemble-averaged pressure P_B is uniform. Each collision between a pair of bubbles produces a local force dipole acting on the fluid. For bubbles m,n that are in contact there is a corresponding local force density

$$\mathbf{f}(\mathbf{x},t) = \mathbf{F}_C^{mn}\left\{\Delta\left(\mathbf{x} - \mathbf{Y}^{(m)}(t)\right) - \Delta\left(\mathbf{x} - \mathbf{Y}^{(n)}(t)\right)\right\} \tag{20}$$

where we use the fact that $\mathbf{F}_C^{mn} = -\mathbf{F}_C^{nm}$ as in (8). In terms of the separation vector between the two bubbles, this is approximately

$$f_i(\mathbf{x},t) = F_{iC}^{mn}\left(Y_j^{(m)} - Y_j^{(n)}\right)\frac{\partial}{\partial x_j}\Delta\left(\mathbf{x} - \left(Y_j^{(m)} + Y_j^{(n)}\right)/2\right) \tag{21}$$

which has the form of a stress tensor with $f_i = \frac{\partial}{\partial x_j}\sigma_{ij}^B$. This bubble stress tensor σ_{ij}^B at any instant is then a sum over all the contacting bubbles. The pressure P_B may be estimated from a volume average over the flow domain as

$$P_B = \left\langle \frac{1}{3}\sigma_{ii}^B \right\rangle \tag{22}$$

$$= \frac{1}{3L^3}\sum_{m=1}^{N}\sum_{n=m+1}^{N} F_{iC}^{mn}\left(Y_i^{(m)} - Y_i^{(n)}\right) \tag{23}$$

The results for the dispersive bubble pressure are given in Table 3 for the void fraction of 6.0%. The pressure is indeed greatest for the largest bubbles and decreases with bubble size, consistent with a decrease in the collision frequency with bubble size. The results are scaled by $\rho\phi^2 u'^2$. The variation within the range of 0.8–1.5 shows that the rms turbulent fluctuation velocity u' is an appropriate choice for the velocity scale in (19).

4. Turbulence modulation

In this section we consider the ways in which the Eulerian characteristics of the fluid flow are modified by the presence of the bubbles or particles. As buoyancy forces are excluded, the main issues are the inertial forces associated with a particle (or bubble), which determine the force monopole, and the stresslet component of the force dipole in response to local velocity gradients, specifically the rate of strain. Both the monopole and the stresslet are associated with the finite volume effect of the particles. Generally, a particle moves with the surrounding fluid (5) and motion relative to an otherwise uniform far-field flow arises from inertial forces for a bubble or solid particle. The finite volume effect of a neutrally buoyant particle is associated with the stresslet. The questions we consider are the length scales at which the particle phase and fluid phase interact and how the evolution of the energy spectrum of the fluid phase is modified by the particles. These interactions may be individual or the collective effect of many particles locally.

We compare several different simulations with bubbles, neutrally buoyant particles and solid slightly inertial particles. The important parameters are collected in Table 2. The single phase flow characteristics are identical on the two grids used (128^3, 192^3) and the turbulent Reynolds number Re_λ stays in the range of 57–60. This is similar to the conditions for the simulations by ten Cate et al. (2004) of inertial particles in homogeneous turbulence. In order to compare directly with these simulations, we simulate a specific configuration $S2$ with solid inertial particles of density $\rho_P = 1.4\rho$. All the particles are small compared to the Taylor microscale but larger than the Kolmogorov dissipation length scale η, with particle radius a varying between 3.8 and 5.6η.

Analyzing the results collected in Table 2, we see that both the turbulent intensity of the flow and the rate of kinetic energy dissipation by viscosity are essentially constant with small variations of 4% for u' and 7% for ϵ. A general comment is that the turbulence intensity in all cases is similar because the forcing parameters are kept constant. The total energy input by the forcing is balanced by the turbulent dissipation rate. This is a particular feature of the simulation where all the scales of the flow are resolved. Departures from this may occur due to limited scale separation between the range of forced wavenumbers and those in the dissipation range or where there is a direct interaction of the particle phase and the forcing scales. In two-way coupling simulations using point particles (Boivin et al., 1998; Squires and Eaton, 1990), the particles act as a sink of turbulent kinetic energy. Unresolved scales of the order of the particle diameter are modeled by an interphase coupling term. The dissipation by the particles is governed by the slip velocity of the particles relative to the local fluid velocity of the resolved part of the flow. In the fully resolved simulations by ten Cate et al. (2004), they also obtained the result that the rate of energy dissipation is constant over the various two-phase flow conditions studied and that this balances the random forcing power input.

In Figs. 3 and 4, we plot the energy spectra resulting from the simulations with the two different sizes of particles, corresponding to scale ratios $a/\eta = 5.5$ ($B1$,$N1$,$S1$) and $a/\eta = 3.9$ ($B2$,$N2$,$S3$). The wavenumbers are scaled by k_d, based on the particle diameter $d = 2a$ and $k_d d = 2\pi$, following the proposal by ten Cate et al. (2004). We observe that the large scale kinetic energy content (low wavenumbers) behave similarly because their dynamics are fixed by the forcing scheme and the level of kinetic energy input at low wavenumbers is essentially the same for all the simulations. We expect that the presence of bubbles or particles will lead to interactions with smaller scales. Indeed, a significant increase of kinetic energy at higher wavenumbers is seen for $k/k_d > 0.78$ for the larger particles ($a = 0.37\lambda$) and $k/k_d > 0.65$ for the smaller particles ($a = 0.26\lambda$). Similar features are obtained in the dissipation

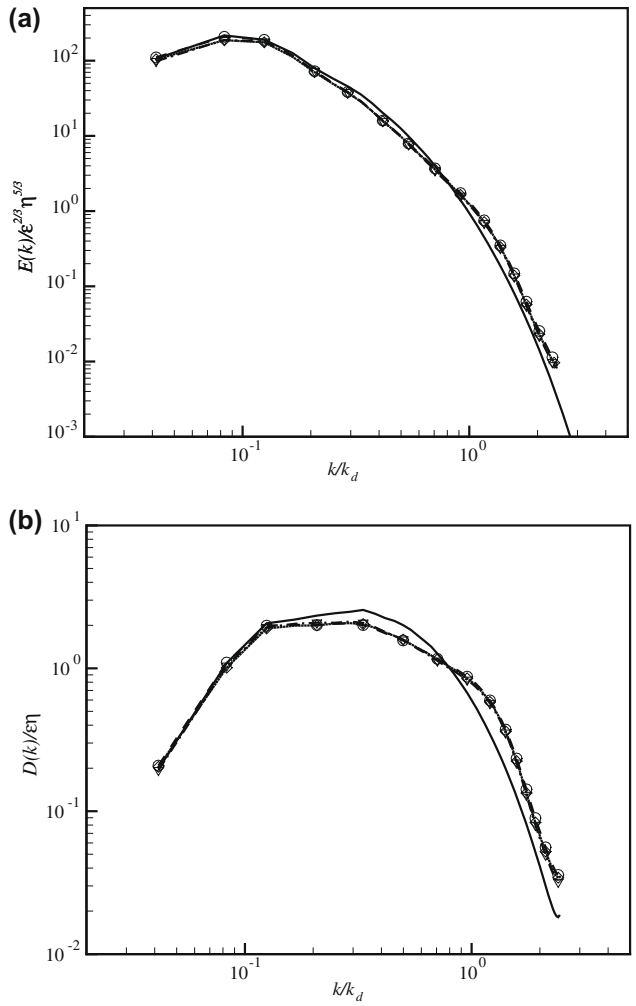

Fig. 3. Energy (a) and dissipation (b) spectra (grid 128^3). Solid line, single phase flow; dashed line with circles, bubbles $B1$; dash dot line with triangles, neutral particles $N1$; dotted line with diamonds, solid particles $S1$.

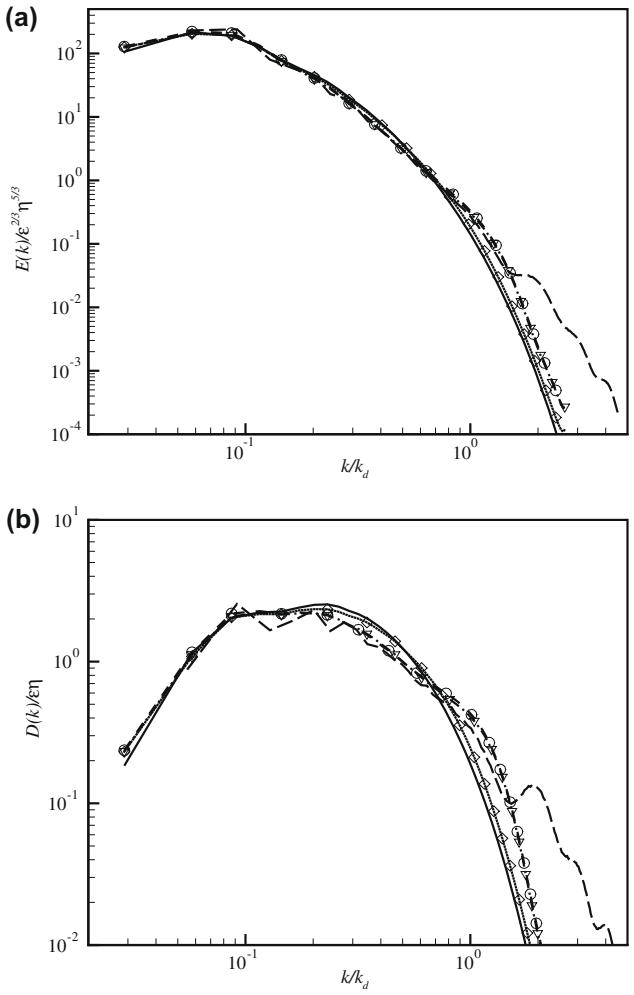

Fig. 4. Energy (a) and dissipation (b) spectra (grid 192^3). Solid line, single phase flow; dashed line with circles, bubbles $B2$; dash dot line with triangles, solid particles $S2$; dotted line with diamonds, solid particles $S2$–M; Long dash line, dataset $S2$ from (ten Cate et al., 2004).

spectra also shown in Figs. 3 and 4. This enhancement is more closely related to finite size effects than momentum transfer as it is seen equally with bubbles, neutrally buoyant and inertial solid particles. Simulations with only the force monopole term lead to only a weak modification of the energy spectrum, see case $S2$–M in Fig. 4. It was unexpected that all three types of particle would induce similar modifications of energy and dissipation spectra regardless of their particular dispersion characteristics and net momentum transfer (monopole). The dynamics instead are more directly controlled by the stresslet contribution. This enforces a zero local rate of strain within the spherical Gaussian envelope so that the flow responds as a solid body within the fluid volume occupied by bubbles or particles. This in turn leads to a significant enhancement of *small scale* kinetic energy and rate of viscous dissipation near each particle surface as local flow variations are deflected around the particle. The local perturbation of the flow by the dispersed phase occurs on the scale of the particle diameter.

At larger scales, $k/k_d < 0.6$, the kinetic energy level is slightly reduced over a range of intermediate wavenumbers. This behavior has already been observed by many authors (Mazzitelli and Lohse, 2003; ten Cate et al., 2004; Boivin et al., 1998) although the physical origins differ. Buoyancy, for example, plays a major role in the studies of Mazzitelli and Lohse (2003). It is important to note that the pivoting wavenumber k_p, where the transition between enhanced and reduced kinetic energy is different when the size of the bubbles changes. ten Cate et al. (2004) investigated distinct configurations varying the volumetric concentration and particle inertia but with constant characteristics of the turbulence ($Re_\lambda = 61$) and a *fixed* particle size $a/\eta = 3.95$. Varying the density ratio and the particle concentration, led to the striking result that the pivoting wavenumber k_p always corresponded to $k_p/k_d = 0.72$. This is very similar to our results, where for case $S2$: $k_p/k_d = 0.65$ and for this particle size the results for $B2$, $N2$ and $S2$ give k_p/k_d clustered around this value.

The question is whether k_d characterizes the value of k_P as the particle size varies. In Fig. 5, we show the dissipation spectra for the neutral particles $N1$ and $N2$ with the wavenumbers scaled now by the Kolmogorov length scale η. Here the pivoting wavenumber is $k_p\eta = 0.45$ for the larger particles ($N1$) and $k_p\eta = 0.56$ for the smaller particles ($N2$). As expected, the value of $k_p\eta$ is larger for the smaller particle, but the increase is only a factor of 1.25 compared to the 1.43 factor for the particle sizes. The observed values of k_p/k_d are 0.78 ($N1$) and 0.68 ($N2$) and these differ by a factor of 0.87. The outcome then is that the scaling of k_p by the particle size is a better correlation than a simple scaling with η but the results are not conclusive. Our values for k_p/k_d bracket those of ten Cate et al. (2004) so there may be fluctuation errors. But it is likely that there is a more subtle Reynolds number effect, based on the particle size, which modifies the correlation with particle size.

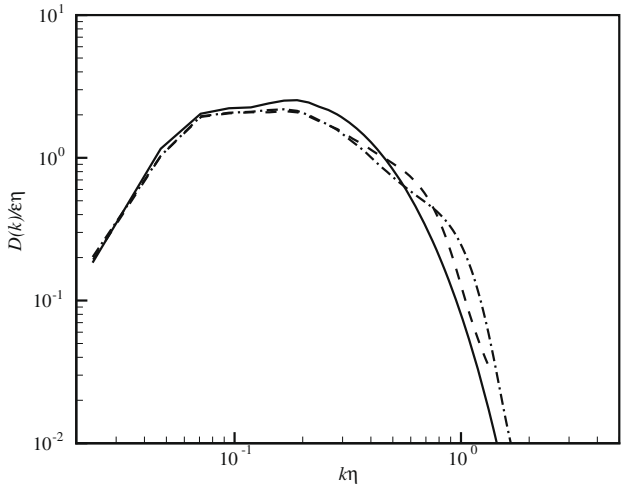

Fig. 5. Dissipation spectra $D(k)$ plotted against wavenumber scaled as $k\eta$: solid line, single phase flow; dashed line, neutral particles $N1$; dash dot line, neutral particles $N2$.

The simulations of ten Cate et al. (2004) were performed using a lattice-Boltzmann approach. In analyzing the energy and dissipation spectra, see Fig. 4, we note that significant oscillations occur in the high wavenumber content that are related to discontinuities in the velocity gradient across particle interfaces. Discontinuities lead to a k^{-4} scaling of the tail of the energy spectrum and k^{-2} for the dissipation spectrum. Although the authors argued that this part of the spectrum contains only 1% of the total energy or dissipation, such oscillations may affect the precise determination of the pivoting wavenumber. There are inherent challenges to measuring and interpreting Fourier spectra in the spatial domain for dispersed two-phase flow. In the present FCM simulations, the spectra remain smooth as the velocity and velocity gradients are continuously defined throughout the whole domain. (Post-processing of the computed volumetric flow field may be used to reconstruct the discontinuous variations.)

As we identify the stresslet as being the main contribution to flow modulation, we consider how this may contribute to the energy transfer between scales. We can use the momentum Eq. (2) and the force decomposition (3) to derive an evolution equation for the energy spectrum $E(k)$ in wavenumber space. Since the flow is statistically stationary, there is a balance of energy input at large scales by the random forcing $F_R(k)$, direct viscous dissipation $D(k)$, the usual nonlinear energy transfer $T(k)$ and the contributions from the force monopoles $M(k)$ and the force dipoles $H(k)$. The latter two depend on the correlation, in spectral space, of the particle body force $\mathbf{f}(\mathbf{x},t)$ and the fluid velocity $\mathbf{u}(\mathbf{x},t)$. The balance is

$$0 = F_R(k) - D(k) + T(k) + M(k) + H(k) \tag{24}$$

where the dissipation spectrum function is $D(k) = 2\nu k^2 E(k)$. The values of $M(k)$ and $H(k)$ can be evaluated directly from the simulation data. First we write

$$f_i^M(\mathbf{x}) = \sum_{n=1}^{N_p} F_i^n \Delta(\mathbf{x} - \mathbf{Y}^n) \tag{25}$$

$$f_i^D(\mathbf{x}) = \sum_{n=1}^{N_p} G_{ij}^n \frac{\partial}{\partial x_j} \Delta'(\mathbf{x} - \mathbf{Y}^n) \tag{26}$$

Then, the monopole $M(k)$ and the dipole energy transfer functions $H(k)$ are defined as

$$M(k) = \sum_{k-\frac{1}{2}\le|\mathbf{k}|<k+\frac{1}{2}} \hat{f}_i^M(\mathbf{k})\hat{u}_i(-\mathbf{k}) \tag{27}$$

$$H(k) = \sum_{k-\frac{1}{2}\le|\mathbf{k}|<k+\frac{1}{2}} \hat{f}_i^D(\mathbf{k})\hat{u}_i(-\mathbf{k}) \tag{28}$$

in which $\hat{\psi}$ is the Fourier coefficient of a variable ψ.

Fig. 6 shows the scaled values of the dissipation spectrum $D(k)$ and dipole energy-transfer spectrum $H(k)$ for the two cases $N1$ and $N2$. The results with bubbles (B) or inertial particles (S) are very similar. The dipole energy-transfer spectrum $H(k)$ shows that the particle stresslets extract energy from large-scale motions and supply it to the small scales.

At low wavenumbers, the dipole contribution acts as an additional dissipation which is consistent with the classical concept of an enhanced effective viscosity in a particulate suspension as noted in Section 2.1. Analogous to the suspension viscosity effect, we define ν_{add} so as to approximate $H(k)$ by $-2\nu_{add}k^2E(k)$ and then

$$D(k) - H(k) = 2\nu_{eff}k^2E(k) = 2(\nu + \nu_{add})k^2E(k) \tag{29}$$

This approximation is used in the low wavenumber range, $k/k_d < 0.3$, to estimate the additional viscosity ν_{add} by scaling $H(k)$ with the dissipation spectra. Table 4 gives ν_{add} for all the simulations. The derived approximations for $H(k)$ are included in Fig. 6, where we compare results for the neutrally buoyant particles. The values of ν_{add} are consistent for the larger particles with the Stokes–Einstein estimate (11) at this volume fraction. However for the smaller particles ($N2$,$S2$) and bubbles ($B2$), the values of ν_{add} are significantly lower. It seems that the additional viscosity is not only dependent on the volumetric concentration but also

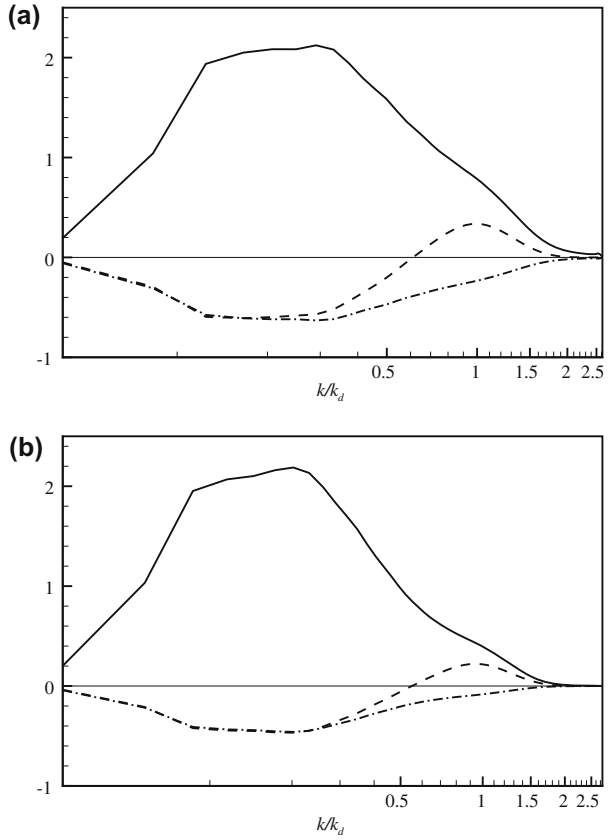

Fig. 6. Determination of the effective viscosity. (a) Solid line, dissipation rate spectra ($N1$); dashed line, dipole energy transfer ($N1$); dash dot line, corresponds to $\nu_{add}/\nu = 0.150$. (b) Solid line, dissipation rate spectra ($N2$); dashed line, dipole energy transfer ($N2$); dash dot line corresponds to $\nu_{add}/\nu = 0.105$.

Table 4
Additional effective viscosity in turbulent two-phase flow simulations.

Case	$B1$	$N1$	$S1$	$B2$	$N2$	$S2$
ν_{add}/ν	0.142	0.154	0.148	0.101	0.108	0.105

on the particle or bubble size. We have no explanation for this at present. There is no inherent reason for the Stokes–Einstein estimate to be applicable here in this inherently unsteady, finite Reynolds number context. Additionally, there is no clear separation of scales between the particle size and the scale on which the velocity gradients vary. This is discussed further in Section 6.

The inertial forces on solid particles ($S1$,$S2$) and the bubbles ($B1$,$B2$) contribute to $M(k)$ and this force monopole spectral energy transfer term similarly extracts energy from low wavenumbers and supplies this at high wavenumbers. Even in the absence of inertial forces, short-range collision forces between neutral particles generate a force monopole contribution $M(k)$. Tests were made to evaluate this and the effect of varying the collision force parameters in (8). For both cases $N1$ and $N2$, there was very little variation in $M(k)$ with the collision parameters and its effect is limited to a narrow range of wavenumbers around $k \sim 0.1k_d$. The values of $M(k)$ are smaller than for $H(k)$. Inertial collisions between particles will contribute to the particle-phase stress acting on the flow and will become more significant at higher concentration levels.

A question may be posed as to whether there is a direct effect of the random forcing of the turbulence on the particle–turbulence dynamics. We did turn off the random forcing in some test cases for a short interval after a statistically stationary state was obtained to see if the correlations would change before the turbulence decayed. By and large there was little difference. For example, some spurious artifacts in the monopole contribution $M(k)$ to the energy spectrum transfer at the lowest wave numbers disappeared. The results for $H(k)$ shown in Fig. 6 did not change.

5. Lagrangian statistics

Further details on the Lagrangian statistics of bubbles, neutrally buoyant and solid particles are now presented for the cases $B1$ to $S2$. Each of the Lagrangian statistics were obtained from ensemble averages over 10^7 trajectories. Table 5 shows the rms fluctuation (in dimensional form) of the particle velocity, V' and the particle acceleration A', together with the corresponding flatness factors, F_V and F_A. The values of V' are only slightly smaller than u' and the flatness factor F_V for all cases is close to 3, indicating that the velocity fluctuations have an essentially Gaussian distribution. The velocity statistics are not sensitive to the type of particle and the values are consistent with the Eulerian statistics.

Unlike the velocity statistics, the acceleration statistics show clear differences. The Lagrangian acceleration is an intermittent quantity and particles may experience large accelerations during the sweeping motion within a vortex, as noted by Porta et al. (2001), Lee et al. (2004) and Yeung et al. (2006a). As bubbles tend to accumulate in the high vorticity regions, the fluctuation levels for the acceleration A' are much larger for the bubbles than the other particles. On the other hand, solid particles tend to accumulate in the low-vorticity (high-strain rate) regions rather than within vortices (Calzavarini et al., 2008), which results in the lowest value of A'. As the inertia of the solid particle is moderate ($\rho_p/\rho = 1.4$), the difference in the statistics between solid and neutrally buoyant particles is weaker than it would be for a gas–solid flow.

Table 5
Lagrangian data following the particles or bubbles for: rms velocity fluctuation, V' ; flatness factor for the velocity fluctuations, F_V ; rms fluctuation in the acceleration, A' ; flatness factor for the acceleration fluctuations, F_A ; rms angular velocity, $\mathbf{\Omega}'$. The last column gives the value of C_0^* , estimated from the maximum values in Fig. 9.

Case	V'	F_V	A'	F_A	$\mathbf{\Omega}'$	C_0^*
$B1$	19.0	2.95	1308.4	6.50	42.7	2.60
$N1$	18.4	2.83	967.7	5.55	33.4	2.07
$S1$	18.1	2.79	857.1	5.19	31.1	1.77
$B2$	19.0	2.95	1400.8	8.07	48.6	2.64
$N2$	19.1	2.84	1145.0	6.66	38.7	2.43
$S2$	18.7	2.81	1023.2	6.24	35.6	2.15

The rms fluctuations in the particle acceleration A' may be compared to the level of values for a Lagrangian fluid tracer. Yeung and Pope (1989) obtained a relation for the acceleration of a tracer particle as $A_T'^2 = 1.92(\epsilon^3/\nu)^{1/2}$ at this Reynolds number. This corresponds to $A_T' = 1508$. The particle accelerations A' for the neutral particles ($N1$) and ($N2$) are significantly less, reflecting the finite size of the particles and the limited response to turbulence on scales smaller than the particle.

The rms fluctuations in the particle angular velocity $\mathbf{\Omega}'$, defined as $\langle \mathbf{\Omega}_1^2 \rangle^{1/2}$ are also consistent with the above description of particles interacting with vortices in the turbulence. The rms data for $\mathbf{\Omega}'$, in Table 5, show similar features for the neutral particles (cases $N1$ and $N2$) and the solid inertial particles (cases $S1$ and $S2$). The neutral particles showed no tendency to accumulate. There is a 6–8% reduction in the values of $\mathbf{\Omega}'$ for the solid particles as compared to neutral particles cases $N1$ and $N2$. The reduction is a weaker effect than the corresponding increase for bubbles. This is in part because the density ratio $\rho_P/\rho = 1.4$ corresponds to slightly inertial particles with $(m_P - m_F)/m_F = 0.4$ while for bubbles this ratio equals -1.

The rms fluctuations in the particle angular velocity $\mathbf{\Omega}'$ may also be compared with those for a Lagrangian tracer particle, which will rotate with an angular velocity equal to half the local fluid vorticity. On this basis, the rms fluctuating angular velocity of a tracer particle would be $\mathbf{\Omega}_T' = 62$. The finite size of a neutrally buoyant particle would, according to (13), reduce this estimate for $\mathbf{\Omega}'$ to 44.5 for ($N1$) and to 50 for ($N2$) using the corresponding dissipation spectra. A further factor is the finite Reynolds number of the particle motion. Poe and Acrivos (1975) demonstrated that the angular velocity of a spherical particle freely suspended in a shear flow is reduced at finite Reynolds number relative to the estimate at zero Reynolds number of half the fluid vorticity. This experimental observation is consistent with numerical simulations (Bagchi and Balachandar, 2002; Wang, 2009). In the present conditions, this would lead to a further reduction of 15–25% in the angular velocity. FCM captures this effect at low Reynolds numbers (Wang, 2009) and the results for $\mathbf{\Omega}'$ for the neutral particles in Table 5 fit this general picture.

The Lagrangian velocity auto-correlation function $\rho_v(t)$ is shown in Fig. 7. The auto-correlations $\rho_v(t)$ for the two different sizes of bubbles are almost identical and decay faster when compared to neutrally buoyant and solids particles at early time ($t/\tau_K < 15$). However, later $t/\tau_K > 15$, the rate of decay for neutrally buoyant particles becomes similar to bubbles, while $\rho_v(t)$ of solid particles is always larger than the two others. Once trapped in a vortex, bubbles move toward the vortex core exhibiting rotational motion that results in the faster decay of $\rho_v(t)$ at early time. The inertial solid particles are swept outside these small-scale structures of the turbulence. As a result, ρ_v decays more slowly as compared to bubbles and neutrally buoyant particles. Collision contacts between bubbles are more likely than between the other particles due to the effects of local accumulations and this would further influence the relative correlation time scales.

Fig. 8 shows the probability density function (pdf) of the acceleration. The pdf has very long tails compared to a Gaussian

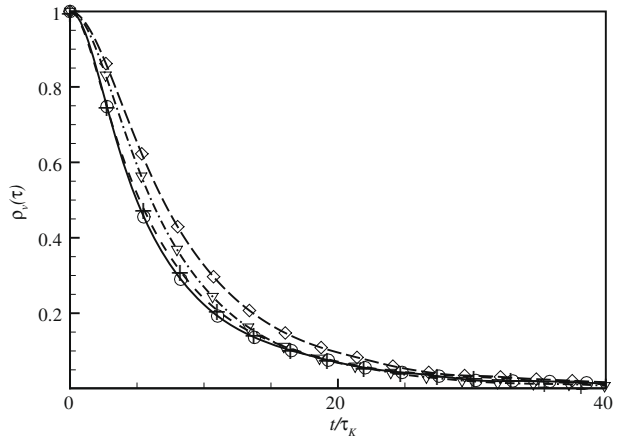

Fig. 7. Velocity auto-correlation function. Solid line with circles, *B*1; dashed line with crosses, *B*2; dash dot line with triangles, *N*1; long dash line with diamonds, *S*1.

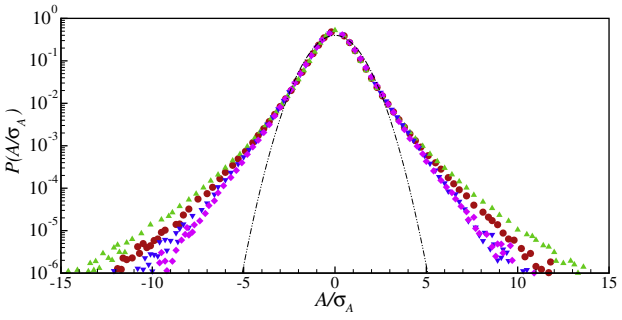

Fig. 8. (Color online) Probability density function of particle acceleration. Legend for symbols: circle, *B*1; triangle, *B*2; nabla, *N*1; diamond, *S*1.

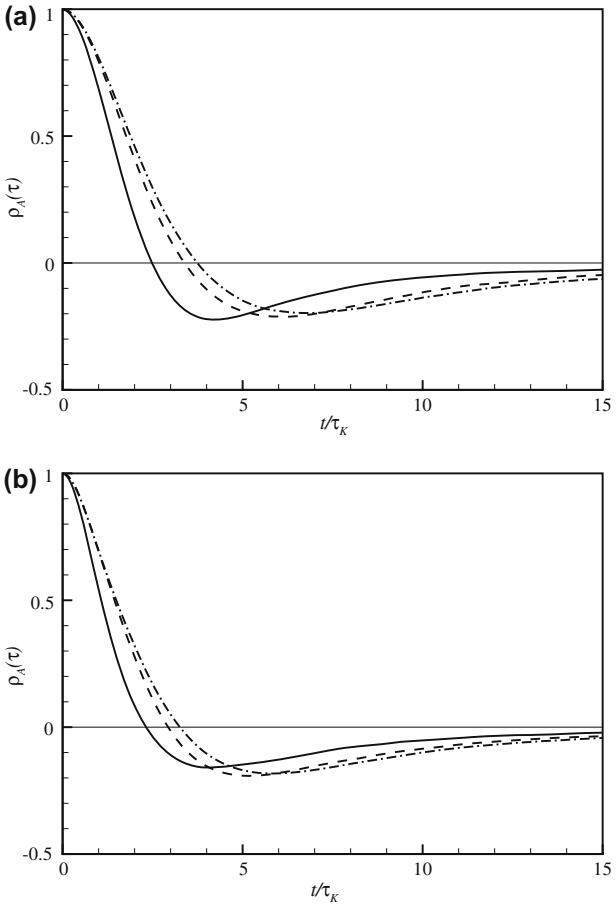

Fig. 9. Acceleration auto-correlation function. (a) Solid line, *B*1; dashed line, *N*1; dash dot line, *S*1. (b) Solid line, *B*2; dashed line, *N*2; dash dot line, *S*2.

distribution indicating a high level of intermittency of the acceleration (Porta et al., 2001) (events of high intensity are more probable than the Gaussian estimate). When scaled by corresponding rms accelerations σ_a the pdf's are very similar in the central region, $|a|/\sigma_a < 3$. This indicates that the differences in the acceleration statistics between the different particles or bubbles, and different sizes, come from the intermittent events, which are closely related to the coherent vortical structures (Lee et al., 2004). These features of the pdf's are consistent with the experimental observations, obtained at higher Reynolds numbers (Qureshi et al., 2007; Volk et al., 2008; Xu and Bodenschatz, 2008).

The Lagrangian acceleration correlation function for fluid tracers is known to decay much faster than the velocity correlation and has zero integral time scale. Yeung and Pope (1989) found that the acceleration auto-correlation crosses zero at about $2\tau_K$ and this varies only slightly with the turbulent Reynolds number. Mordant et al. (2002) showed that the auto-correlation of the acceleration magnitude decays slowly and argued that this long-time correlation is a key feature of intermittency in turbulence. Lee et al. (2004) suggested that this different behavior of acceleration and acceleration magnitude comes from the rotational motion of particles in a vortex in that the zero-crossing time of the acceleration auto-correlation is related to the rotational time scale of a particle as it is swept around in a vortex.

The acceleration auto-correlation function $\rho_A(t)$ is presented in Fig. 9. The zero-crossing time of the auto-correlation function for smaller bubbles (*B*1) and larger bubbles (*B*2) are, respectively, 2.33 and $2.50\tau_K$. These values are smaller than for neutrally buoyant and solid particles. At early times $(t < 2\tau_K)$, $\rho_A(t)$ for the neutrally buoyant and the solid particles are only slightly different. Due to the effects of inertia, $\rho_A(t)$ for the solid particles decays more slowly than for the neutrally buoyant particles. Both Volk et al. (2008) and Xu and Bodenschatz (2008) have measured the acceleration auto-correlations for a range of isolated particles and particle sizes at high Reynolds numbers. The first zero-crossing for bubbles, $a/\eta = 4.4$, is earlier than for neutral or denser particles and for larger neutrally buoyant particles, $a/\eta = 7.4$ the auto-correlation extends further (Volk et al., 2008). Both observations are consistent with the present simulations but it is not possible to make a quantitative comparison.

Finally we examine the Lagrangian velocity structure function. Fig. 10 shows the velocity structure function $D_L(t)$,

$$D_L(t) = \langle (V(s+t) - V(s))^2 \rangle \tag{30}$$

where $D_L(t)$ is normalized by ϵt. In a high Reynolds number inertial sub-range $D_L(t)/\epsilon t$ would be a constant C_0. The results shown for the two different sizes of bubbles are similar. For both neutrally buoyant and solid particles, the maximum value of $D_L(t)$ is greater for the smaller particle size while the time at which the maximum is attained is shorter. For the present simulations there is no inertial sub-range as the Reynolds number is too low. From the normalized velocity structure function, we can provisionally evaluate C_0^* as a low Reynolds number analog to the Kolmogorov constant C_0 (Yeung and Pope, 1989; Sawford, 1991) for comparison purposes. Estimates of C_0^* are given in Table 5, based on the maximum values shown in Fig. 10. The estimates of C_0^* for the bubbles (cases *B*1 and *B*2) are about 2.6, which is similar to that of a fluid particle (Yeung and Pope, 1989). The peak value for the bubbles is observed at approximately $4.3\tau_K$.

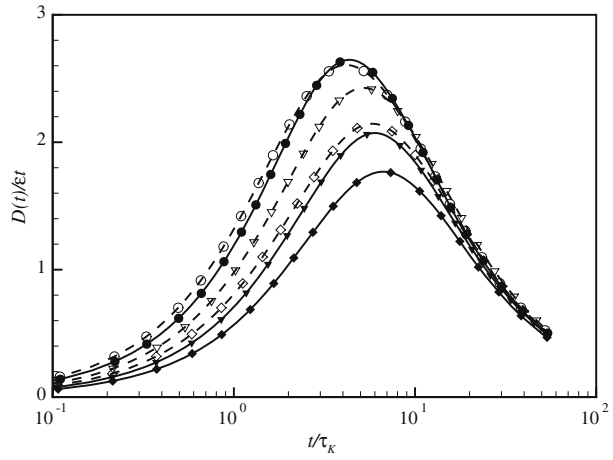

Fig. 10. Normalized velocity structure function. Solid line with solid circles, *B*1; solid line with solid triangles, *N*1; solid line with solid diamonds, *S*1; dashed line with open circles, *B*2; dashed line with open triangles, *N*2; dashed line with open diamonds, *S*2.

6. Conclusions

In this paper we have examined a number of issues relating to the dynamics of finite size particles at low to moderate volume fractions in liquid–solid or liquid-bubble turbulence. The results for the dissipation spectra in Section 4 show that the particles enhance the small scale turbulence at length scales below the particle size. This is determined primarily by the finite size of the particle and not by the specific density of the particle. The scaling of the pivoting wavenumber k_P by the particle diameter, through k_d, as proposed by ten Cate et al. (2004), is consistent with the present results but does not fully match them. There may be an additional dependence for example on d/η.

In describing the dynamics of the energy spectra, it would appear possible to represent the transfer of energy from large scales to small scales by the particle phase through the use of an effective suspension viscosity, at least for scales substantially larger than the particle. The characteristics of this viscosity are more complex than a simple application of the Stokes–Einstein result for dilute suspensions. There is limited fundamental information at present on the rheology of particle suspensions at finite Reynolds numbers. Recent numerical simulations by Kulkarni and Morris (2008) for neutrally buoyant particles in a steady Couette flow indicate that the Stokes–Einstein estimate should still apply at volume fractions of 5%.

The contribution $H(k)$ from the force dipoles to the spectral energy transfer in (24) represents a sum over the stresslet components of all the particles. The particle contribution to the bulk stress in a finite Reynolds number flow depends not only on this but also a local volume average of the symmetric moments of the particle accelerations and a Reynolds stress term (Batchelor, 1970; Kulkarni and Morris, 2008). The latter is for the smaller-scale disturbance flow around each particle relative to the local volume averaged flow velocity. In the present formulation these other terms are included in the nonlinear inertial transfer term $T(k)$.

The effective viscosity of viscous suspension flows depends too on the relative positions of particles and localized concentrations of particles should have an observable effect (Hinch, 1977). In the present context, the bulk concentration of 6%, or less, is still relatively low and such effects may be limited as seen in the small variation of v_{eff} in Table 4, even though the bubbles and solid particles have some tendency to cluster. The dynamics of viscous suspensions are governed by the velocity fluctuations created by the disturbance flows of the individual particles randomly dispersed in the flow and the correlations between these flows is important. Particle suspensions in turbulent flow are subject to the underlying turbulence and the correlations of the disturbance flows with the turbulence are more significant.

The Lagrangian statistics of the particle motion have also been investigated. At finite volume fractions, collisions and contact forces between particles (or bubbles) will inherently limit local accumulations and the "collisional pressure" will contribute to the particle-phase stress. This pressure will also enhance particle dispersion if there are spatial variations in the mean concentration. In other respects, in homogeneous systems, the collisions will limit the correlation times for the particle motion. These effects will increase significantly with particle concentration.

There is evidence too for the spatial filtering effect from the finite particle size on the response to the turbulent motion. For example, for a neutrally buoyant particle, this is a function of the particle size relative to the Kolmogorov scale, or to the Taylor microscale. As indicated in (16), the Stokes number *St* is closely related to the ratio of the particle size to the Taylor microscale. Similarly the ratio τ_P/τ_K is closely related to the ratio of the particle size to the Kolmogorov length scale. The present simulations are at too low a Reynolds number to establish an inertial sub-range but the particle diameters are 7–11 times larger than the Kolmogorov scales and so fall within the transition range described by (Qureshi et al., 2007). This is in addition to any inertial response linked to the specific density of the particle.

These results given here are preliminary in many respects and we hope that they will stimulate future work to explore these issues more fully.

Acknowledgments

This work was supported by a grant of HPC resources from the Arctic Region Supercomputing Center at the University of Alaska Fairbanks as part of the Department of Defence High Performance Computing Modernization Program. Support by DARPA under the Friction Drag Reduction Program (ATO) is gratefully acknowledged. (The content of this paper does not necessarily reflect government policy and no official endorsement should be inferred). E.C. acknowledges the CNRS for funding the international program of collaboration PICS #3419. The authors wish to thank Dr. Andreas ten Cate for providing the numerical data on the spectra from ten Cate et al. (2004).

References

Abbas, M., 2008. Auto-diffusion de particules dans un ecoulement cisaille: Des interactions hydrodynamiques aux effets collisionnels. Ph.D. thesis, Institut National Polytechnique de Toulouse.
Bagchi, P., Balachandar, S., 2002. Effect of free rotation on the motion of a solid sphere in linear shear flow at moderate Re. Phys. Fluids 14, 2719–2737.
Batchelor, G., 1967. An Introduction to Fluid Dynamics. Cambridge University Press.
Batchelor, G., 1970. The stress system in a suspension of force-free particles. J. Fluid Mech. 41, 545–570.
Batchelor, G., 1988. A new theory of the instability of a uniform fluidized bed. J. Fluid Mech. 193, 75–110.
Batchelor, G., Green, J., 1972. The hydrodynamic interaction of two small freely-moving spheres in a linear flow field. J. Fluid Mech. 56, 375–400.
Boivin, M., Simonin, O., Squires, K., 1998. Direct numerical simulation of turbulence modulation by particles in isotropic turbulence. J. Fluid Mech. 375, 235–263.
Brunk, B., Koch, D., Lion, L., 1998. Turbulent coagulation of colloidal particles. J. Fluid Mech. 364, 81–113.
Calzavarini, E., Kerscher, M., Lohse, D., Toschi, F., 2008. Dimensionality and morphology of particle and bubble clusters in turbulent flow. J. Fluid Mech. 607, 13–24.
Campbell, C., 1990. Rapid granular flows. Ann. Rev. Fluid Mech. 22, 57–92.
Climent, E., Maxey, M., 2003. Numerical simulations of random suspensions at finite reynolds numbers. Int. J. Multiphase Flow 29, 579–601.
Dance, S., Climent, E., Maxey, M., 2004. Collision barrier effects on the bulk flow in a homogeneous random suspension. Phys. Fluids 16, 828–831.

Dance, S., Maxey, M., 2003. Incorporation of lubrication effects into the force-coupling method for particulate two-phase flow. J. Comput. Phys. 189, 212–238.
Dong, S., Xu, J., Maxey, M., Karniadakis, G., 2005. Microbubble dynamics in turbulent channel flow. In: 2nd International Symposium on Seawater Drag Reduction, Busan, Korea.
Druzhinin, O., Elghobashi, S., 1999. On the decay rate of isotropic turbulence laden with microparticles. Phys. Fluids 11, 602–610.
Elghobashi, S., Truesdell, G., 1993. On the two-way interaction between homogeneous turbulence and dispersed solid particles. Part I: turbulence modification. Phys. Fluids 5, 1790–1801.
Eswaran, V., Pope, S., 1988. An examination of forcing in direct numerical simulations of turbulence. Comput. Fluids 16, 257–278.
Ferrante, A., Elghobashi, S., 2004. On the physical mechanisms of drag reduction in a spatially-developing turbulent boundary layer laden with bubbles. J. Fluid Mech. 503, 345–355.
Ferrante, A., Elghobashi, S., 2005. Reynolds number effect on drag reduction in a microbubble-laden spatially developing turbulent boundary layer. J. Fluid Mech. 543, 93–106.
Hinch, E., 1977. An averaged-equation approach to particle interactions in a fluid suspension. J. Fluid Mech. 83, 695–720.
Hwang, W., Eaton, J., 2006. Homogeneous and isotropic turbulence modulation by small heavy (St $\sim$50) particles. J. Fluid Mech. 564, 361–393.
Jeong, J., Hussain, F., 1995. On the identification of a vortex. J. Fluid Mech. 285, 69–94.
Kawamura, T., Kodama, Y., 2002. Numerical simulation method to resolve interactions between bubbles and turbulence. Int. J. Heat Fluid Flow 23, 627–638.
Kiger, K., Pan, C., 2002. Suspension and turbulence modification effects of solid particulates on a horizontal turbulent channel flow. J. Turbul. 3, N19.
Kulkarni, P., Morris, J., 2008. Suspension properties at finite Reynolds number from simulated shear flow. Phys. Fluids 20, 040602.
Lance, M., Bataille, J., 1991. Turbulence in the liquid phase of a uniform bubbly air–water flow. J. Fluid Mech. 222, 95–118.
Lee, C., Yeo, K., Choi, J.-I., 2004. Intermittent nature of acceleration in turbulence. Phys. Rev. Lett. 92, 144502.
Liu, D., Maxey, M., Karniadakis, G., 2002. A fast method for particulate microflows. J. Microelectromech. Syst. 11, 691–702.
Lomholt, S., Maxey, M., 2003. Force coupling method for particles sedimenting in a channel: Stokes flow. J. Comput. Phys. 184, 381–405.
Lomholt, S., Stenum, B., Maxey, M., 2002. Experimental verification of the force coupling method for particulate flows. Int. J. Multiphase Flow 28, 225–246.
Lu, J., Fernandez, A., Tryggvason, G., 2005. The effect of bubbles on the wall shear in a turbulent channel flow. Phys. Fluids 17, 095102.
Magnaudet, J., Eames, I., 2000. The motion of high Reynolds number bubbles in inhomogeneous flows. Ann. Rev. Fluid Mech. 32, 659–708.
Maxey, M., 1987. The motion of small spherical particles in a cellular flow field. Phys. Fluids 30, 1915–1928.
Maxey, M., 1999. Examples of fluid–particle interactions in dispersed two-phase flows. In: Paper AIAA 99-3691, 30th AIAA Fluid Dynamics Conference, Norfolk, VA.
Maxey, M., Liu, D., Dong, S., Karniadakis, G., 2006. New advances in force-coupling method: from micro to macro. In: Balachandar, S., Prosperetti, A. (Eds.), Proceedings of IUTAM Symposium on Computational Approaches to Disperse Multiphase Flow. Springer, pp. 237–246.
Maxey, M., Patel, B., 2001. Localized force representations for particles sedimenting in Stokes flow. Int. J. Multiphase Flow 27, 1603–1626.
Mazzitelli, I., Lohse, D., 2003. The effect of microbubbles on developed turbulence. Phys. Fluids 15, L5–L8.
Mazzitelli, I., Lohse, D., Toschi, F., 2003. On the relevance of the lift force in bubbly turbulence. J. Fluid Mech. 488, 283–313.
Minev, P., Lange, U., Nandakumar, K., 1999. A comparative study of two-phase flow models relevant to bubble column dynamics. J. Fluid Mech. 394, 73–96.
Mordant, N., Delour, J., Levque, E., Arneodo, A., Pinton, J.-F., 2002. Long time correlations in lagrangian dynamics: a key to intermittency in turbulence. Phys. Rev. Lett. 89, 254502.
Murai, Y., Fukuda, H., Oishi, Y., Kodama, Y., Yamamoto, F., 2007. Skin friction reduction by large air bubbles in a horizontal channel flow. Int. J. Multiphase Flow 33, 147–163.
Poe, G., Acrivos, A., 1975. Closed-streamline flows past rotating single cylinders and spheres: inertia effects. J. Fluid Mech. 72, 605–626.
Pope, S., 2000. Turbulent Flows. Cambridge University Press.
Porta, A.L., Voth, G., Crawford, A., Alexander, J., Bodenschatz, E., 2001. Fluid particle accelerations in fully developed turbulence. Nature 409, 1017–1019.
Qureshi, N., Bourgoin, M., Baudet, C., Cartellier, A., Gagne, Y., 2007. Turbulent transport of material particles: an experimental study of finite size effects. Phys. Rev. Lett. 99, 184502.
Rensen, J., Luther, S., Lohse, D., 2005. The effects of bubbles on developed turbulence. J. Fluid Mech. 538, 153–187.
Sanders, W., Winkel, E., Dowling, D., Perlin, M., Ceccio, S., 2006. Bubble friction drag reduction in a high-Reynolds-number flat-plate turbulent boundary layer. J. Fluid Mech. 552, 353–380.
Sawford, B., 1991. Reynolds number effects in Lagrangian stochastic models of dispersion. Phys. Fluids A 3, 1577–1586.
Squires, K., Eaton, J., 1990. Particle response and turbulence modification in isotropic turbulence. Phys. Fluids A 2, 1191–1203.
Sundaram, S., Collins, L., 1997. Collision statistics in an isotropic particle-laden turbulent suspension. Part 1: direct numerical simulation. J. Fluid Mech. 335, 75–109.
Sundaram, S., Collins, L., 1999. A numerical study of the modulation of isotropic turbulence by suspended particles. J. Fluid Mech. 379, 105–143.
Taylor, G., 1921. Diffusion by continuous movements. Proc. Lond. Math. Soc. 20, 196–212.
ten Cate, A., Derksen, J., Portela, L., van den Akker, H., 2004. Fully resolved simulations of colliding monodisperse spheres in forced isotropic turbulence. J. Fluid Mech. 519, 233–271.
van den Berg, T., Luther, S., Lathrop, D., Lohse, D., 2005a. Drag reduction in bubbly Taylor-Couette turbulence. Phys. Rev. Lett. 94, 044501.
van den Berg, T., Luther, S., Lohse, D., 2005b. Energy spectra in microbubbly turbulence. Phys. Fluids 18, 038103.
van den Berg, T., Luther, S., Mazzitelli, I., Rensen, J., Toschi, F., Lohse, D., 2006. Turbulent bubbly flow. J. Turbul. 7, N14.
Volk, R., Calzavarini, E., Verhille, G., Lohse, D., Mordant, N., Pinton, J.-F., Toschi, F., 2008. Acceleration of heavy and light particles in turbulence: comparison between experiments and direct numerical simulations. Physica D 237, 2084–2089.
Voth, G., La Porta, A., Crawford, A., Alexander, J., Bodenschatz, E., 2002. Measurement of particle accelerations in fully developed turbulence. J. Fluid Mech. 469, 121–160.
Wang, L.-P., 2009. Private communication.
Wang, L.-P., Maxey, M., 1993a. The motion of microbubbles in a forced isotropic and homogeneous turbulence. Appl. Sci. Res. 51, 291–296.
Wang, L.-P., Maxey, M., 1993b. Settling velocity and concentration distribution of heavy particles in homogeneous isotropic turbulence. J. Fluid Mech. 256, 27–68.
Xu, H., Bodenschatz, E., 2008. Motion of inertial particles with size larger than Kolmogorov scale in turbulent flows. Physica D 237, 2095–2100.
Xu, J., Maxey, M., Karniadakis, G., 2002. Numerical simulation of turbulent drag reduction using micro-bubbles. J. Fluid Mech. 468, 271–281.
Yeo, K., Maxey, M., 2010. Simulation of concentrated suspensions using the force coupling method. J. Comput. Phys., in press.
Yeung, P., Pope, S., 1989. Lagrangian statistics from direct numerical simulations of isotropic turbulence. J. Fluid Mech. 207, 531–586.
Yeung, P., Pope, S., Lamorgese, A., Donzis, D., 2006a. Acceleration and dissipation statistics of numerically simulated isotropic turbulence. Phys. Fluids 18, 065103.
Yeung, P., Pope, S., Sawford, B., 2006b. Reynolds number dependence of Lagrangian statistics in large numerical simulations of turbulence. J. Turbul. 7, N58.
Yoshimoto, H., Goto, S., 2007. Self-similar clustering of inertial particles in homogeneous turbulence. J. Fluid Mech. 577, 275–286.
Zenit, R., Hunt, M., Brennen, C., 1997. Collisional particle pressure measurements in solid–liquid flows. J. Fluid Mech. 353, 261–283.
Zhang, Z., Prosperetti, A., 2005. A second-order method for three-dimensional particle simulation. J. Comput. Phys. 210, 292–324.